Multicomponent Aerosol Dynamics of the Pb-O_2 System in a Bench Scale Flame Incinerator

Wen Y. Lin, Virendra Sethi, and Pratim Biswas*
Department of Civil and Environmental Engineering,
University of Cincinnati,
Cincinnati, OH 45221-0071

A study was carried out to understand the formation and growth of lead particles in a flame incinerator. A bench scale flame incinerator was used to perform controlled experiments with lead acetate as a test compound. A dilution probe in conjunction with real-time aerosol instruments was used to measure the evolution of the particle size distribution at different locations in the flame region. A multicomponent lognormal aerosol model is developed accounting for the chemistry of the lead-oxygen system, and various aerosol dynamic phenomena such as nucleation, coagulation, and condensation. Reasonable agreement is obtained between the predictions of the model using appropriate kinetic parameters and the experimental results.

INTRODUCTION

Incineration of hazardous wastes is emerging as an important treatment method prior to disposal. It serves to destroy the organic content of the wastes by thermal oxidation, thereby reducing the bulk volume and the toxicity of the treated wastes for ultimate disposal. Although the method offers application to a varied stream of wastes, its acceptance still remains questioned primarily because of a lack of understanding of the physical and chemical characteristics of the gaseous and particulate emissions from such units. Several studies on particulate emissions from combustion sources clearly indicate an enrichment of volatile metal species on submicrometer-sized particles. These enriched particles are both toxic and in the inhalable size range, and therefore present a potential health hazard (Davison et al., 1974). Most particulate control devices have poor collection efficiencies in this submicrometer size range, and a lack of understanding of the process results in noncompliance with the stipulated regulations (Federal Register, 1982; Oppelt, 1986, 1987).

Studies show that waste incineration and coal combustion are the two major contributors to atmospheric loading of toxic metals such as antimony (Sb), arsenic (As), cadmium (Cd), selenium (Se), vanadium (V), lead (Pb), and zinc (Zn) (Kowalczyk et al., 1978). The particles formed are about 0.02 μm in diameter and grow by condensation of vapor or coagulation with other particles to cover a 0.02–1.0-μm size range in the exhaust (Gladney et al., 1976; Lee, 1988; Smith et al., 1979; Kauppinen and Pakkanen, 1990).

A number of studies have been undertaken in the past to assess the relationship of particle composition and particle size from emission data available from coal combustors (Davison et al., 1974; Gladney et al., 1976) and waste incinerators in operation (Greenberg et al., 1978; Law and Gordon, 1979; Bennett and Knapp, 1982). Flagan and Friedlander (1971) and

* To whom correspondence should be addressed.

Aerosol Science and Technology 17:119–133 (1992)

0278-6826/92/$5.00

Damle et al. (1982) reviewed the formation of particles in coal combustion and have proposed condensation of vaporized species as a probable mechanism for the formation of submicrometer-sized particles. It is also well recognized from samples that the submicrometer-sized particles are preferentially enriched with volatile metal species such as antimony, lead, cadmium, silver, copper and zinc (Davidson et al., 1974; Gladney et al., 1976). Vogg et al. (1986) reported enrichment factors of 20 for Pb, 60 for Sb, 100 for Cd, and 600 for Hg in emissions of municipal waste incinerators.

In a recent study on hospital waste incineration by Kauppinen and Pakkanen (1990), a bimodal mass size distribution of particulate emissions was observed. The 0.1–0.2-μm diameter fine mode accounted for 7% to 74% of Pb, 62% to 77% of Cd, and 20% to 80% of Zn of the total particulate phase, indicating evaporation and reformation of fine particles for the volatile species.

Waterland et al. (1990) have performed pilot scale tests in a rotary kiln, using volatile and nonvolatile trace metal feeds. The results of the study support the influence of temperature, chlorine content, and the volatility of the metallic species in the enrichment in the submicrometer mode. However, no detailed size distributions for the submicrometer sized particles are reported.

Mulholland and Sarofim (1991) have studied the effect of temperatures on the partitioning of particles between submicrometer, intermediate, and residual phases. An increase in the submicron phase was reported for higher temperatures.

Barton et al. (1988) have carried out an analytical study to predict the fate of toxic metals in waste incinerators. They have concluded that the partitioning of metals during incineration is sensitive to temperature history in the incinerator, chlorine content of the wastes, entrained particle size, residence time, and cooling rates downstream of the combustors. In another study, Lee (1988) has suggested a thermodynamic approach to predict the chemical and physical form of each species present in the combustion chamber.

Graham et al. (1990) have initiated a compositional mapping of emissions from combustion of coal and residual oils. X-ray microanalysis has been used for the study to establish the condensation mechanism and history for the metals present in the ash. A need for further work in the area of multicomponent condensation, and gas phase kinetics for the prediction of ash structure is reported.

The focus of most of the studies till now, with the exception of that by Graham et al. (1990), Kauppinen and Pakkanen (1990), and Mulholland and Sarofim (1991), has been the assessment of trends from samples of particles greater than about 0.5 μm collected from incinerators and coal combustors in operation. The following observations are made by all workers: Metallic species are more concentrated in the suspended particles than in the captured flyash owing to size dependence of the enrichment factor; concentration of metal species is dependent on the temperature history, waste feed composition, and the presence of other species in the incinerator environment; Sb, As, Cu, Pb, Ag, and Zn are the toxic metals found concentrated on particles <1.0 μm in diameter.

Better ways of estimating incinerator emissions are needed to improve design and sizing of particulate control devices and to determine the impact of the emissions on the air quality (Oppelt, 1987; Grosshandler, 1990). There is also a need for predictive models that would estimate the emissions from a given incinerator system and thereby reduce costs for conducting metal emissions testing in the field (Lee, 1988).

As a first step towards development of such a predictive model, it was necessary to study the extent of effect of key parameters in a simple controlled study. Sethi and Biswas (1990a) have developed a theoretical model for particle formation and growth in a flame incinerator and studied the effects of vapor feed rates and the presence of seed particles on the evolution of the particle size distribution. Further development of the model to include other parameters and its application to pilot and full-scale operations necessitated an experimental validation of the model in its simplest form.

An experimental study was carried out to verify the prediction of the proposed model. A bench scale flame torch has been used to incinerate lead acetate. A description of the experimental setup and the results are presented. The model developed earlier by Sethi and Biswas (1990a) is extended to include oxidation kinetics and multicomponent (lead and lead oxide) aerosol dynamics, and the predictions are compared to the experimental data.

EXPERIMENTAL METHOD

The schematic diagram of the experimental set up is shown in Figure 1. A multiport quartz burner was used to obtain a steady, soot-free cylindrical flame by choice of an appropriate fuel-air ratio (Table 1). Methane-air flames with different premix ratios were studied to choose a suitable flame length for the experiment. The following criteria was used in making the choice: steady flame with no lift-off, clear sootless flame, and peak temperature in the range 900–1300°C as in a typical incinerator operation. In this work, a ratio of 1:2.5 was selected to get a flame length of ~12 cm and a Reynolds number at the jet inlet (Re_i) of 496. A type R, Rh-Pt thin wire (0.002 in. in diameter) thermocouple was used to measure the temperatures along the flame axis (Figure 2). Lead acetate

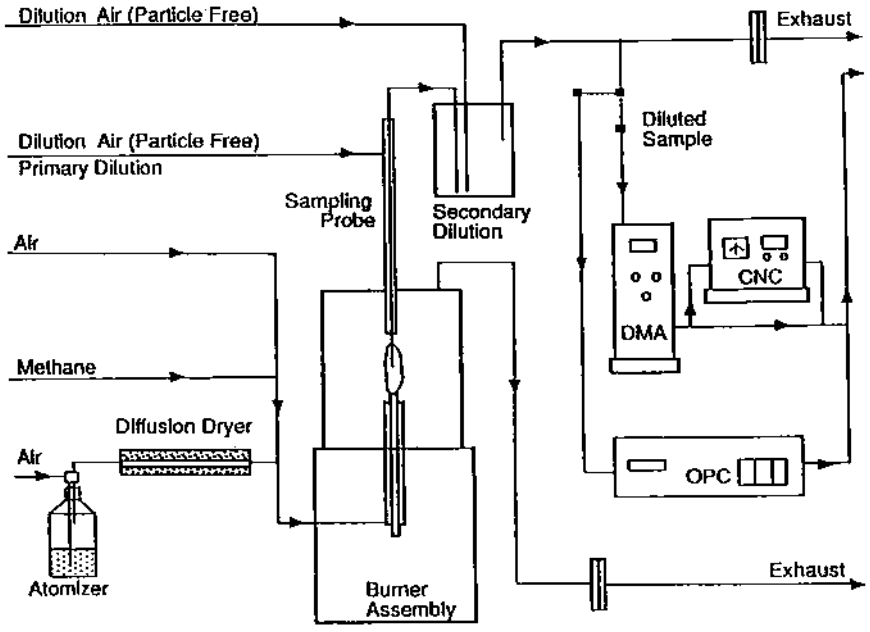

FIGURE 1. Schematic diagram of the experimental setup.

TABLE I. List of Experimental Conditions

Flame	
Flow rate CH_4: air (L/min)	1:2.5
Flame length (cm)	12
Fuel	Methane
Inlet temperature of gases (°K)	298
Ambient temperature (°K)	298
Jet diameter, d_j (cm)	0.2
Lead feed	
Atomizer feed solution	
Lead acetate-trihydrate (g/mL)	0.159
Atomizer air flow rate (L/min @35psi)	2.5
Feed aerosol (lead equivalent)	
Number concentration, N_0(no./cm^3)	2×10^6
Geometric mean volume, v_g(cm^3)	5.62×10^{-15}
Geometric standard deviation, σ_g	1.43

was selected as the test compound to study the formation of particles from a volatile metal species. High solubility in water and low decomposition temperature (~200°C) were the two main properties that made lead acetate an ideal choice. An aqueous solution of lead acetate was atomized using an atomizer (Model 3076, TSI, Inc., St. Paul, MN) The aerosol was then passed through a diffusion dryer to obtain a dry aerosol. The aerosol was premixed with methane and introduced with the fuel mixture. The characteristics of the feed aerosol were determined by sampling from the jet inlet, with no flame. The sample aerosol was measured using a differential mobility particle sizer (DMA Model 3071, CNC Model 3030, TSI, Inc.)

A sampling probe was used to obtain particulate samples from the flame region and convey them to the particle measuring instruments. The probe was designed to minimize losses (Sethi, 1990) and was based on a design described by Biswas et

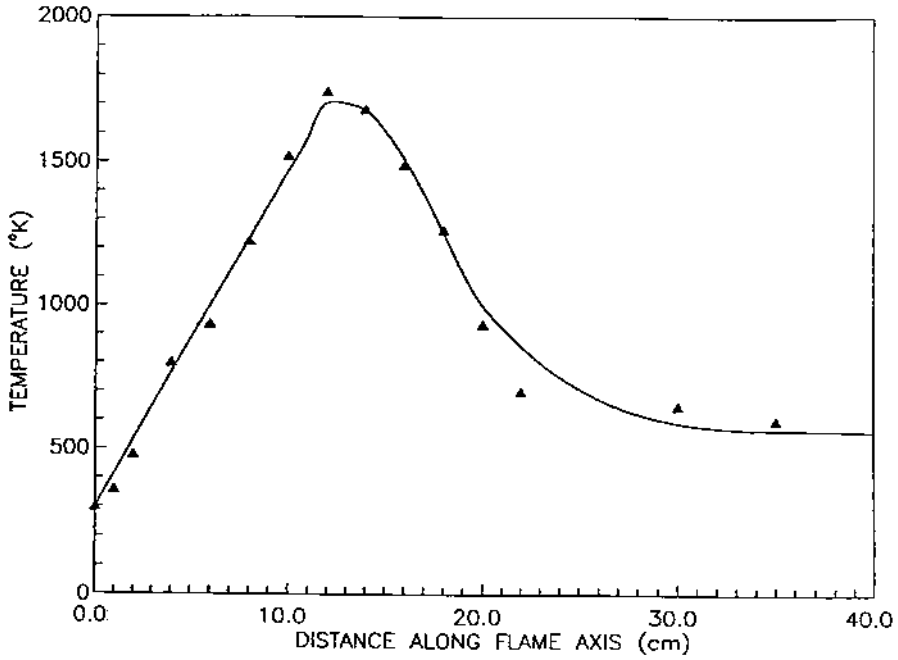

FIGURE 2. Temperature profile as a function of axial distance in the flame. Solid line is fit to experimental data (▲) given by eq. 1.

al. (1989). Chemical reactions and aerosol dynamics were quenched by appropriate dilution with particle-free air. The losses due to anisokinetic sampling were calculated to be insignificant for the particles under study (Stokes number, $Stk << 0.01$) (Hinds, 1982).

The sample intake was calibrated with a fixed dilution air feed and a fixed exhaust flow rate. The flows were left unchanged throughout the course of the experiment. The exhaust gas was passed through a filter prior to exhaust into the fume hood.

A differential mobility particle sizer (DMPS) was used to determine the particle size distribution of the sample aerosols. Measurements were also made using an optical particle counter (OPC, Model LAS-X, PMS, Boulder, CO) and the two measurements compared well for particles >0.1 μm—the lower measurable limit of the OPC (Sethi, 1990).

THEORETICAL MODEL

Lead acetate decomposes rapidly under high temperature conditions, and hence the following reaction of lead and oxygen is considered in the model:

$$2Pb_{(g)} + O_2 \underset{k_-}{\overset{k_+}{\rightleftharpoons}} 2PbO_{(g)}.$$

$PbO_{2(g)}$ is not included in the analysis as it is known to decompose at 290°C (CRC, 1988). Super saturation conditions for the vapors (lead and lead oxide) are obtained due to vapor formation by chemical reaction or due to a temperature decrease downstream of the flame. The super saturated lead and/or lead oxide vapors may either nucleate to form new particles or condense onto existing particles. Further particle growth may also take place due to coagulation.

The temperature history in the flame needs to be determined to use the model equations described later. The expression describing the temperature profile in a diffusion flame is able to predict peak temperatures well but does not predict the axial position of the peak accurately when compared to experimental data (Sethi and Biswas, 1990b). Hence, the simulation is done using a polynomial function to fit the experimentally measured temperature profile shown in Figure 2:

$$\begin{aligned} T &= 273.64 + 117.05x \qquad 0 \le x \le 12 \\ T &= -518.91 - 1.20x + 67.09x^2 \\ &\quad -6.61x^3 + 0.22x^4 - 0.0025x^5 \\ &\qquad 12 \le x \le 19.5 \\ T &= 5364.03 - 398.98x + 11.01x^2 \\ &\quad -0.10x^3 \qquad x \ge 19.5 \end{aligned} \tag{1}$$

The general dynamic equation (GDE) describes aerosol formation and growth by various mechanisms (Friedlander, 1977). Moment forms of this equation have been used, and solution techniques developed by assuming the size distribution to be described by a lognormal function (Lee and Chen, 1984; Pratsinis, 1988; Biswas et al., 1989). Experimental results (Figure 3) indicate that the size distribution can be reasonably described by a unimodal lognormal function. Sethi and Biswas (1990a) have used the lognormal model to predict evolution of the particle size distribution in a diffusion flame. The moment forms of the general dynamic equation for multiple components (Pb and PbO) are developed and described below.

The rate of change of the zeroeth moment, M_0 (particle number concentration), is given as:

$$\rho \frac{\mathrm{d}}{\mathrm{d}t}(M_0/\rho) = I_{\mathrm{Pb}} + I_{\mathrm{PbO}} - \xi M_0^2. \tag{2}$$

The first two terms on the right-hand side (RHS) account for particle formation by nucleation from Pb and PbO vapors, respectively, and the third term for the re-

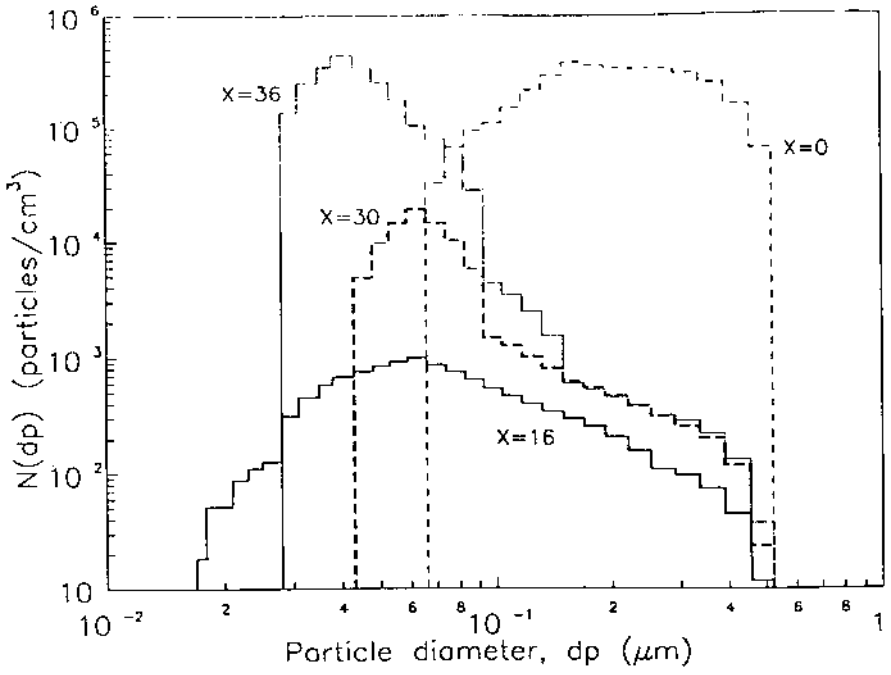

FIGURE 3. Aerosol size distributions measured at four different locations in the flame: (a) $x = 0$ cm, (b) $x = 16$ cm, (c) $x = 30$ cm, and (d) $x = 36$ cm from the burner inlet.

duction of the particle number concentration due to coagulation. The variables are described in the Nomenclature. The rate of change of the first moment, M_1 (total aerosol volume), is given as:

$$\rho\frac{\mathrm{d}}{\mathrm{d}t}(M_1/\rho) = \{Iv^* + \eta M_0\}_{\mathrm{Pb}} + \{Iv^* + \eta M_0\}_{\mathrm{PbO}}. \quad (3)$$

The first term in the first bracket on the RHS accounts for the increase in aerosol volume due to the formation of the nucleated particles, and the second term in the first bracket accounts for volume change by condensation or evaporation. The two brackets account for the contribution from lead and lead oxide, respectively. The rate of change of the second moment, M_2, is given as:

$$\rho\frac{\mathrm{d}}{\mathrm{d}t}(M_2/\rho) = \{Iv^{*2} + 2\epsilon M_1\}_{\mathrm{Pb}} + \{Iv^{*2} + 2\epsilon M_1\}_{\mathrm{PbO}} + 2\zeta M_1^2. \quad (4)$$

The first term in the first brackets on the RHS accounts for the change due to nucleation, and the second term in the bracket for the effect of condensation or evaporation. The two brackets account for the contribution from lead and lead oxide respectively. The last term on the RHS accounts for changes due to particle coagulation.

The rates of change of the lead and lead oxide vapor concentrations, determined by a vapor balance accounting for chemical reaction and aerosol dynamics,

are given as:

$$\rho\frac{\mathrm{d}}{\mathrm{d}t}([\mathrm{Pb}]/\rho) = -2k_+[\mathrm{Pb}]^2[\mathrm{O_2}] + 2k_-[\mathrm{PbO}]^2 - \frac{\{Iv^* + \eta M_0\}_{\mathrm{Pb}}\rho_{\mathrm{Pb}}}{Mw_{\mathrm{Pb}}}. \quad (5)$$

and

$$\rho\frac{\mathrm{d}}{\mathrm{d}t}([\mathrm{PbO}]/\rho) = 2k_+[\mathrm{Pb}]^2[\mathrm{O_2}] - 2k_-[\mathrm{PbO}]^2 - \frac{\{Iv^* + \eta M_0\}_{\mathrm{PbO}}\rho_{\mathrm{PbO}}}{Mw_{\mathrm{PbO}}}. \quad (6)$$

The first two terms on the RHS account for the chemical reaction of the vapors, and the terms in the brackets account for the change due to nucleation and condensation/evaporation. To compute the nucleation and condensation rates, the saturation ratio of the vapors must be computed. This is done by solving the vapor balance Eqs. 5 and 6 to obtain the concentration of the vapor (lead or lead oxide) and dividing by the saturation concentration computed using the vapor pressure—temperature data for Pb and PbO (CRC, 1988) at the local temperature obtained from Eq. 1.

Eqs. 2–6 constitute a set of coupled ordinary differential equations that are solved using the Adams-Moulton routine, DIVPAG (IMSL, 1987). The axial location at any time t is determined by using the velocity expression in the laminar cylindrical jet (Sethi and Biswas, 1990a). The initial conditions for M_0, M_1 and M_2 are determined from the lead acetate aerosol feed, expressing them in terms of an equivalent quantity of lead. Lead and lead oxide vapors are assumed to be absent at the inlet (initial vapor concentration = 0). The classical nucleation theory rate expression is used (Friedlander, 1977). The moment form of the coagulation and condensation coefficients are described in the Nomenclature. No detailed information on the kinetic rate constants (k_+, k_-) for the oxidation of lead was available, other than the activation energy ($E_a = 40$ kcal/mol; Iofe et al., 1977). A combination of collision reaction rate theory (Moore and Pearson, 1981) and thermodynamic data is used to compute the reaction rate constants for the chemical reactions and the values are listed in Table 2. A sensitivity calculation on the effect of varying the reaction rate constant on the predicted aerosol parameters is also carried out.

Entrainment of the ambient air into the cylindrical jet lowers the concentration of the vapor and particulate species in the flame. The entrainment velocity, v_δ, at the jet boundary is given by (Kanury, 1982)

$$v_\delta = u_i\frac{4}{Re_i}\left\{1 + \frac{48x}{Re_i d_i}\right\}^{-1}. \quad (7)$$

The total volume of the ambient air entrained, Q_{ent}, into the jet volume upto an axial position x_j is thus given by

$$Q_{ent} = \int_0^{x_j} v_\delta(2\pi\delta)\,\mathrm{d}x = 4\pi\nu x_j. \quad (8)$$

As the entrained air has a certain size distribution ($M_{0a} = 1.0 \times 10^5$ particles cm^{-3} air, $M_{1a} = 1.24 \times 10^{-10}$ cm^3 cm^{-3} air and $M_{2a} = 8.7 \times 10^{-25}$ cm^6 cm^{-3} air), the kth moment of the aerosol distribution at a location "$j+1$" is given by

$$M_k^{j+1} = M_k^j\left\{\frac{Q_{in} + 4\pi\nu x_j}{Q_{in} + 4\pi\nu x_{j+1}}\right\} + M_{ka}\left\{\frac{4\pi\nu(x_{j+1} - x_j)}{Q_{in} + 4\pi\nu x_{j+1}}\right\}. \quad (9)$$

TABLE 2. Parameters for Computation of Rate Constants for the $2Pb_{(g)} + O_2 \rightleftharpoons 2PbO_{(g)}$ Reaction Using the Collision Rate Theory and Thermodynamic Data

$k_+ = A_+ \exp(-E_a/RT)$, $\quad$ mol^{-2}·cm^6·s^{-1}

For trimolecular reactions (Moore and Pearson, 1981)

$$A_+ = 8\pi^{3/2}(2K_B T)^{1/2}(2r_{Pb})^2(r_{Pb} + r_{O2})^2\delta \cdot\{(2/m_{Pb})^{1/2} + (1/m_{Pb} + 1/m_{O_2})^{1/2}\} \cdot N_{av}^2 e^{1/2}, \quad \text{mol}^{-2}\cdot\text{cm}^6\cdot\text{s}^{-1}$$

Using thermodynamic criteria

$A_+/A_- = (RT)^{-\Delta n}\exp(\Delta S/R)$
$E_a = 40$ kcal/mol$(= 1.68 \times 10^{12}$ ergs/mol)
(Iofe et al., 1977)
$m_{Pb} = 3.44 \times 10^{-22}$g
$m_{O2} = 5.32 \times 10^{-23}$g
$\Delta n = -1$
$N_{av} = 6.0238 \times 10^{23}$ no./mol
$r_{Pb} = 1.97$ Å
$r_{O2} = 1.48$ Å
$\delta \sim 10^{-8}$ cm
$R = 8.314 \times 10^7$ erg mol^{-1} °K^{-1}
$\Delta S = -40 \times 10^7$ erg °K^{-1} mol^{-1}

where Q_{in} is the inlet flow rate of the gases into the burner. The predicted number and volume concentrations are computed using Eq. 9 to obtain the diluted values that are observed experimentally at any location x.

RESULTS AND DISCUSSION

A lead acetate solution is used with an atomizer and diffusion dryer to get a stable dry lead aerosol. When a low solution concentration is used in the atomizer, small particles that enter the flame vaporize instantaneously, but at the same time result in a smaller total lead feed into the flame. An optimum quantity of feed aerosol is needed such that the particle size is small enough to assure complete decomposition and vaporization of lead acetate particles, and at the same time, have sufficiently high concentration to cause super saturation conditions in the postcombustion zone. A solution concentration of 0.159 g/mL is used in this study. A shroud is used in order to prevent external draught and obtain a steady flame. Measurements of particle size distributions are made along the axis of the 12-cm flame using a DMPS.

Typical size distributions measured at the inlet ($x = 0$), 16, 30, and 36 cm from the inlet are shown in Figure 3. Size distribution measurements are made at 14 axial locations along the centerline, with at least three measurements at each location. The average of these measurements expressed as the number concentration, volume concentration, volume average diameter, and geometric standard deviation is plotted in Figures 4, 5, 6, and 7 respectively. The vertical bars indicate the range of data obtained, the spread being small in all cases except the measurement at 35 cm. The measurements indicate that the feed aerosol evaporates in the first 10 cm of the flame as the temperature increases (Figure 2). The number concentration drops from 10^6 to 10^4 particles cm^{-3} and not to zero as ambient air is entrained into the flame (Figure 4). Similarly, the volume concentration drops from 10^{-8} to 10^{-11} (Figure 5). There is a slight decrease in the average volume diameter, however, this is not very apparent as the feed aerosol mean size is only slightly larger than that of the ambient air (Figure 6). The measured geometric standard deviation tends to increase as shown in Figure 7. The model prediction up to 20 cm, shown by the solid line, qualitatively agrees with the data, however indicates a sharp drop in number and volume concentrations at $\sim$6 cm ($T = 920$°K). Reasonable agreement is also obtained between 6 and 20 cm, and the aerosol is primarily from the entrained ambient air. At a distance of $\sim$34 cm from the inlet, there is an increase in the measured particle number concentration probably due to new particle formation by nucleation, and an increase in volume concentration due

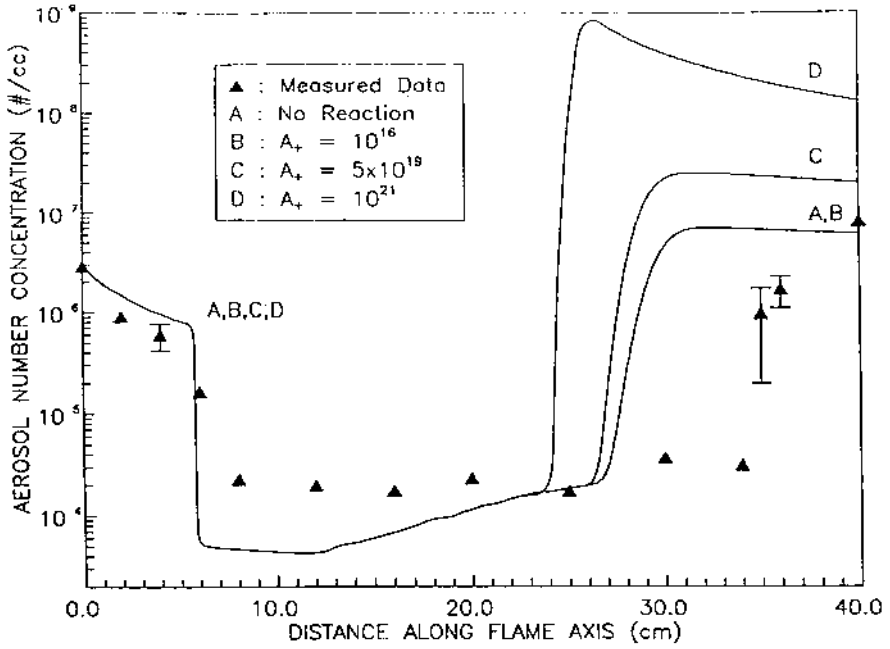

FIGURE 4. Variation of aerosol number concentration with distance along the flame axis at the centerline. Symbols (▲) are measured data and solid lines are model predictions for different choices of the preexponent multiplying term, A_+: (A) no reaction; (B) $A_+ = 10^{16}$ mol^{-2} cm^{-6} s^{-1}; (C) $A_+ = 5 \times 10^{19}$; (D) $A_+ = 10^{21}$.

to both nucleation and growth by condensation. The volume average diameter (Figure 6) decreases beyond 34 cm, and can be explained due to the formation of a large number of small particles by nucleation. The geometric standard deviation also indicates an increase, and this is due to coagulation accompanied with nucleation leading to an increased polydispersity. Measurements are not taken at further distances downstream as the streamlines are not well defined, and hence the expected plateau in the number concentration curve is not observed.

The data indicates that there is a delay between the drop in temperature ($x = 20$ cm) and the onset of nucleation ($x = 34$ cm). This is probably due to the critical saturation ratio being high for lead ($\sim$13 at 1200°K) particles due to the relatively high surface tension value. This delay has interesting implications in the control of metal emissions and is discussed later. The model predictions beyond $x = 20$ cm deviate from experimental data and this is explained in the following paragraphs.

A sensitivity analysis is carried out by varying the reaction rate constant and the results are shown in Figures 4 through 7 and Table 3. The activation energy for the oxidation of lead to lead oxide has been reported to be 40 kcal/mol (Iofe et al., 1977). No values of the pre-exponent multiplying term, A_+, have been reported, and this was computed to be 10^{16} mol^{-2} cm^{-6} s^{-1} (Table 2) for the oxidation of lead to lead oxide using the collision rate theory (Moore and Pearson,

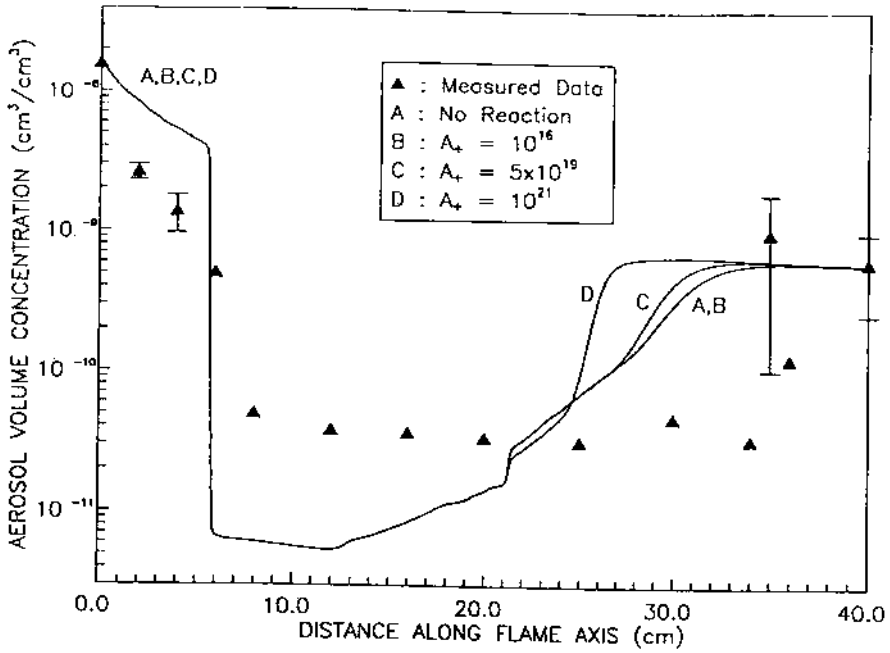

FIGURE 5. Variation of aerosol volume concentration with distance along the flame axis at the centerline. Symbols (▲) are measured data and solid lines are model predictions for different choices of the pre-exponent multiplying term, A_+: (A) no reaction; (B) $A_+ = 10^{16}$ mol^{-2} cm^{-6} s^{-1}; (C) $A_+ = 5 \times 10^{19}$; (D) $A_+ = 10^{21}$.

1981). Two other values of A_+ of 5×10^{19} and 10^{21} are also used for a sensitivity study. There is a slightly increase in the predicted particle size at about $x = 21$ cm (Figure 6), owing to condensation of vapors on the entrained particles from ambient air. For the predictions with faster reaction rates (curves C and D, Figure 6), the size increase is diminished as condensation of lead competes with the chemical reaction of lead to form lead oxide. When the temperature drops further downstream, there is an increase in saturation ratio, and new particles are formed by nucleation. In all cases, the contribution to the total aerosol volume is primarily by condensation (Table 3). This is expected due to the increase in saturation ratio resulting from the drop in temperature, and as soon as some particles are formed further growth is primarily by condensation. As indicated in Table 3 (last column), when a higher value of the chemical reaction rate constant (higher A_+) is used, more of lead oxide is predicted in the final aerosol. Also, for fast reaction conditions (curves C and D, Figure 4), nucleation of lead oxide vapors are predicted at distances closer to the inlet ($\sim$24 and 26 cm, respectively). The predicted mean size of the particles decreases at onset of nucleation as the newly formed particles are small. The geometric standard deviation curves exhibit similar behavior depending on whether nucleation accompanied with coagulation (increase in σ_g) or condensation (decreases in σ_g) is occurring.

The surface tension values of lead and

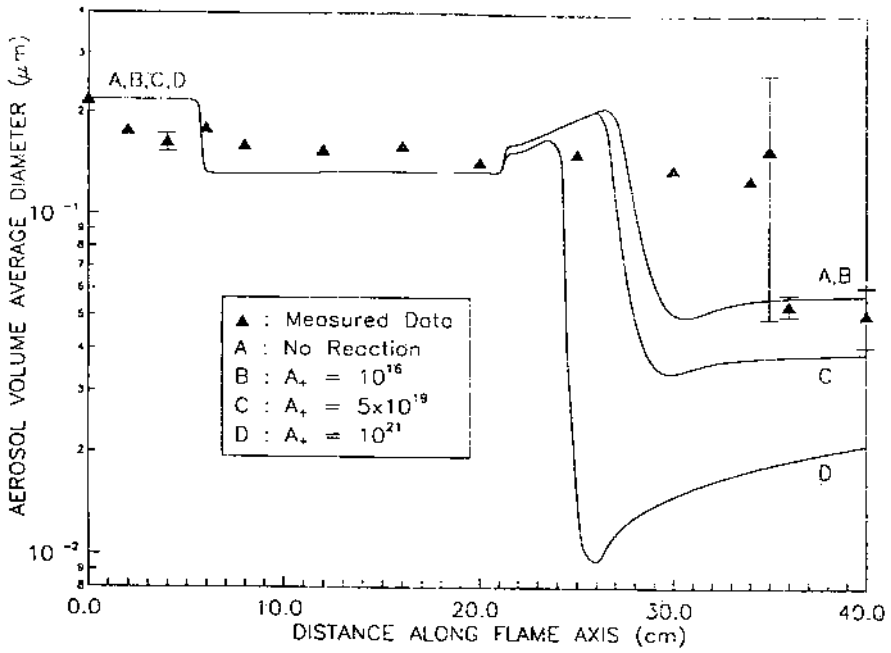

FIGURE 6. Variation of the volumetric mean size with distance along the flame axis at the centerline. Symbols (▲) are measured data and solid lines are model predictions for different choices of the pre-exponent multiplying term, A_+: (A) no reaction; (B) $A_+ = 10^{16}$ mol^{-2} cm^{-6} s^{-1}; (C) $A_+ = 5 \times 10^{19}$; (D) $A_+ = 10^{21}$.

lead oxide are 444 and 250 dyn/cm, respectively (*Comprehensive Inorganic Chemistry,* 1973; *Gmelin Handbuch,* 1969). The lower surface tension of lead oxide implies that there is a lower energy barrier for lead oxide to form stable clusters; hence this tends to reduce the average particle size. The early onset of nucleation for conditions with higher reaction rate constants is a direct consequence of this phenomena.

On comparing the experimental data to model predictions, it appears that the slow reaction rate predictions (curves A and B, Figure 4) seem to describe the data best. The prediction of the onset of nucleation is earlier as compared to the experimental observations, and this may be due to the inadequacy of the classical nucleation theory to predict nucleation rates accurately for the Pb-PbO system, or that the aerosol instruments cannot detect the onset of nucleation very accurately, this being observed in studies with silica particle formation (Biswas et al., 1989). The use of a higher surface tension value (500 dyn/cm) pushes the predicted number concentration curve to the right resulting in a better match with experimental data, however this does not alter the predicted aerosol volume curve significantly. The best agreement is thus obtained for slow oxidation rates (the literature reported value of $E_a = 40$ kcal/mol and $A_+ = 10^{16}$ mol^{-2} cm^{-6} s^{-1}, computed using the collision rate theory, curve B). The resulting ratio of PbO/Pb in the final aerosol is 8×10^{-6}.

These results have an implication on

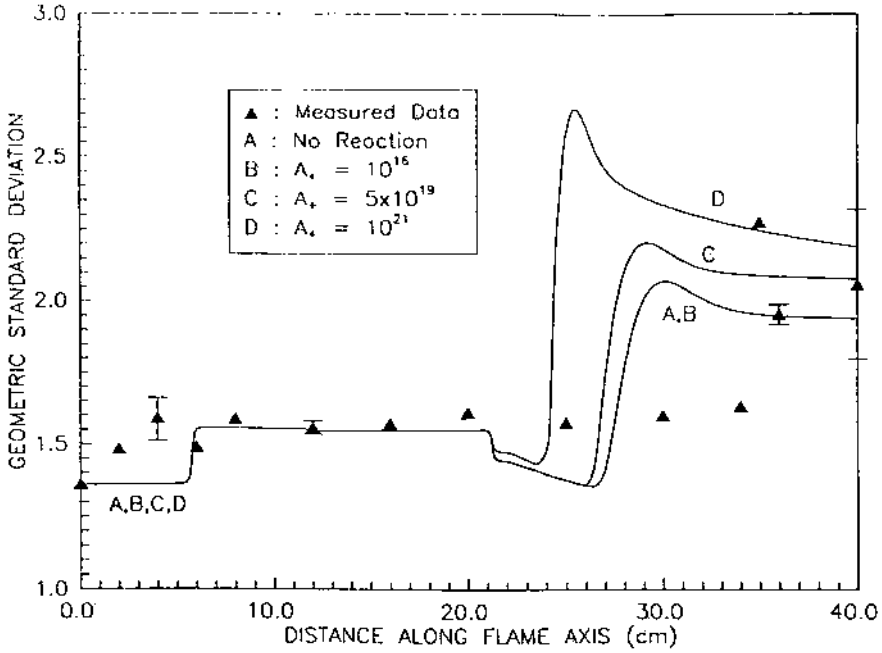

FIGURE 7. Variation of the geometric standard deviation with distance along the flame axis at the centerline. Symbol (▲) are measured data and solid lines are model predictions for different choices of the pre-exponent multiplying term, A_+: (A) no reaction; (B) $A_+ = 10^{16}$ mol^{-2} cm^{-6} s^{-1}; (C) $A_+ = 5 \times 10^{19}$; (D) $A_+ 10^{21}$.

the formation of the submicrometer aerosol mode in incinerators. The presence of chlorine (commonly encountered in waste incinerators; Fournier et al., 1991) leading to the formation of halides and the formation of oxides of metals by oxidation, result in more volatile species being present in the incinerator as compared to the presence of the metal itself. Also, the degree of differences in surface tension of these species has a direct bearing on the sizes of particles formed by nucleation. Because of the delay between the temperature drop and the nucleation of metallic species (as indicated earlier), possible schemes to control the temperature profile to condense out the metallic vapors on other particles and growing them to larger sizes may be an effective way of minimizing the formation of the submicrometer mode.

CONCLUSIONS

A bench scale flame incinerator has been used to study the evolution of the lead–lead oxide aerosol size distribution using a dilution sampling probe and differential mobility particle sizer. The measurements indicate that submicrometer-sized particles were formed in the cool downstream regions of the flame by nucleation of vapors. A multicomponent model accounting for chemical reaction and aerosol dynamics was developed, and reasonable agreement was obtained with

TABLE 3. Predicted Values of the Aerosol Size Distribution Parameters for Different Choices of Chemical Reaction Rate Constants

		dpv (μm)	σ_g	M_0 (no./mL)	M_t (mL/mL)	M_1,Pb (mL/mL)	M_1,PbO (mL/mL)	Contribution to M_1 by				M_1,PbO / M_1,Pb
								Nucleation		Condensation		
								Pb	PbO	Pb	PbO	
A	No Rxn	0.058	1.942	6.09E6	6.13E-10	5.75E-10	0	6.98E-16	0	5.75E-10	0	0
B	A + = 1E + 16	0.058	1.942	6.09E6	6.13E-10	5.75E-10	4.60E-15	6.98E-16	5.16E-34	5.75E-10	4.60E-15	8.00E-6
C	A + = 5E + 19	0.039	2.079	1.98E7	6.13E-10	5.72E-10	3.07E-12	1.70E-16	1.37E-15	5.72E-10	3.07E-12	5.37E-3
D	A + = 1E + 21	0.021	2.191	1.29E8	6.23E-10	5.29E-10	5.68E-11	3.08E-23	1.02E-13	5.29E-10	5.67E-11	1.07E-1

experimental observations. A sensitivity analysis was also performed by varying the chemical reaction rate leading to different ratios of lead and lead oxide, and aerosol size distributions of the aerosol. Key parameters that governed the evolution of the aerosol size distribution were the temperature history in the system, chemical reaction rates, and surface tensions of the various species. It is also recommended that the chemical composition of the particles be determined to verify the model predictions.

Partial support for this work was provided by National Science Foundation Grant CBT 8808813 and Environmental Protection Agency Contract RTP 42.0.

NOMENCLATURE

A preexponent multiplying term in rate constant (mol^2 cm^{-6} s^{-1})

b_0 $0.633 + 0.092\sigma^2 - 0.022\sigma^3$

b_2 $0.39 + 0.5\sigma - 0.214\sigma^2 + 0.029\sigma^3$

B_1 $(36\ \pi)^{1/3} v_1 n_s (K_B T/2\pi m_1)^{1/2}$

B_3 $(48\ \pi^2)^{1/3} \lambda v_1 n_s (8K_B T/\pi m_1)^{1/2}/3$

B_2 $(3/4\ \pi)^{1/6} (6K_B T v_1/m_1)^{1/2}$

B_4 $2K_B T/3m_1$

d jet diameter at inlet (cm)

dpv volume mean diameter (μm)

E_a activation energy

I Nucleation rate (particles cm^{-6} s^{-1}); (Friedlander, 1977)

$$= 2\left\{\frac{P_1}{(2\pi m K_B T)^{1/2}}\right\}(n_1 v_m^{2/3}) \cdot \left\{\frac{\gamma v_m^{2/3}}{K_B T}\right\}^{1/2} \cdot \exp\left\{-\frac{16\pi\gamma^3 v_m^2}{3(K_B T)^3 (\ln S)^2}\right\}.$$

k chemical reaction rate constant (mol^2 cm^{-6} s^{-1})

K_B Boltzmann's constant (1.38×10^{-16} erg °K^{-1})

m molecular mass

M_k kth aerosol moment with respect to particle volume
Mw molecular weight
n number of molecules of monomer species
Δn difference in number of moles between products and reactants
N_{av} Avogadro number
Q flow rate (cm^3/s)
r radius of molecule
R universal gas constant
Re Reynolds number
S saturation ratio
ΔS entropy change associated with reaction
t time (second)
T temperature (°K)
u axial velocity (cm/s)
v^* volume of cluster (cm^3)
v_δ entrainment velocity at jet boundary ($cm\ s^{-1}$)
v_m molecular volume
x distance from burner inlet (cm)

Greek Letters

δ collision distance of molecules
λ mean free path (cm)
ν kinematic viscosity (cm^2/s)
σ geometric standard deviation
ρ density (g/cm^3)
γ surface tension (dyn/cm)
ϵ condensation coefficient, $\epsilon_{FM}\epsilon_C/(\epsilon_{FM}+\epsilon_C)$; (Pratsinis, 1988)

$$\epsilon_{FM} = 2\,B_1 v_g^{2/3} \exp(8\ln^2\sigma)$$

$$\epsilon_C = 2B_3 v_g^{1/3} \exp(7/2\ln^2\sigma)$$

η condensation coefficient, $\eta_{FM}\eta_C/(\eta_{FM}+\eta_C)$; (Pratsinis, 1988)

$$\eta_{FM} = B_1 v_g^{2/3} \exp(2\ln^2\sigma)$$

$$\eta_C = B_3 v_g^{1/3} \exp(1/2\ln^2\sigma).$$

ξ coagulation coefficient, $\xi_{FM}\xi_C/(\xi_{FM}+\xi_C)$; (Pratsinis, 1988)

$$\xi_{FM} = b_0 B_2 v_g^{1/6}\{\exp(25/8\ln^2\sigma) + 2\exp(5/8\ln^2\sigma) + \exp(1/8\ln^2\sigma)\}$$

$$\xi_C = B_4\{1 + \exp(\ln^2\sigma) + 1.257\lambda r_g^{-1}\cdot\exp(1/2\ln^2\sigma)[1 + \exp(2\ln^2\sigma)]\}$$

ζ coagulation coefficients, $\zeta_{FM}\zeta_C/(\zeta_{FM}+\zeta_C)$; (Pratsinis, 1988)

$$\zeta_{FM} = 2b_2 B_2 v_g^{1/6} \exp(3/2\ln^2\sigma)\cdot\{\exp(25/8\ln^2\sigma) + 2\exp(5/8\ln^2\sigma) + \exp(1/8\ln^2\sigma)\}$$

$$\zeta_C = 2B_4\{1 + \exp(\ln^2\sigma) + 1.257\lambda r_g^{-1}\exp(-1/2\ln^2\sigma)\cdot[1 + \exp(-2\ln^2\sigma)]\}$$

Subscripts

a air
ent entrainment
g geometric mean
i inlet
j axial position
k kth moment of aerosol with respect to volume: $k = 0$, aerosol number concentration; $k = 1$, volume concentration; $k = 2$, second volume moment
1 monomer
Pb lead
PbO lead oxide
s saturation
+ forward reaction to form PbO
− reverse reaction to form Pb and O_2
δ boundary layer thickness of the jet

REFERENCES

Barton, R. G., Maly, P. M., Clark, W. D., and Seeker, W. R. (1988). Presented at ASME 13th National Waste Processing Conference, Philadelphia, May 1–4.

Bennett, R. L., and Knapp, K. T. (1982). *Environ. Sci. Technol.* 16:831.

Biswas, P., Li, X., and Pratsinis, S. E. (1989). *J. Appl. Phys.* 65:2445–2450.

Comprehensive Inorganic Chemistry. (1988). Pergamon Press, Oxford, vol. 2, p. 109.

CRC Handbook of Chemistry and Physics, 68th ed. (1988). CRC Press, Inc., Boca Raton, FL.

Damle, A. S., Ensor, D. S., and Ranade, M. B. (1982). *Aerosol Sci. Technol.* 1:119.

Davison, R. L., Natusch, D. F. S., Wallace, J. R., and Evans, C. A. (1974). *Environ. Sci. Technol.* 8:1107.

Federal Register (1982). 47:27516–35.

Flagan, R. C., and Friedlander, S. K. (1971). In *Recent Developments in Aerosol Science.* John Wiley & Sons, New York, Chapter 2.

Fournier, D. J., Whitworth, W. E., Lee, J. W. and Waterland, L. R. (1991). EPA/600/S2-90/043. Risk Reduction Engineering Laboratory, Cincinnati, OH.

Friedlander, S. K. (1977). *Smoke Dust and Haze.* John Wiley & Sons, New York.

Gladney, E. S., Small, J. A., Gordon, G. E., and Zoller, W. H. (1976). *Atmos. Environ.* 10:1071.

Gmelin Handbuch, (1969). *Der Anorganischen Chemie.* Verlag Chemie, GmBH, Weinheim/Bergstr., Teil C —Lieferung 1, p. 72.

Graham, K. A., Walsh, P. M., Beer, J. M., and Sarofim, A. F. (1990). Presented at AAAR Annual Meeting, Philadelphia, p. 224.

Greenberg, R. R., Zoller, W. H., and Gordon, G. E. (1978). *Environ. Sci. Technol.* 12:566.

Grosshandler, W. L. (1990). *Hazard. Waste Hazard. Mater.* 7:1.

Hinds, W. C. (1982). *Aerosol Technology.* Wiley-Interscience, New York, p. 190.

IMSL. (1987). "Problem-Solving Software Systems," International Mathematical and Statistical Libraries, User's Manual, p. 640.

Iofe, L. N., Novoselova, N. A., and Khodakov, G. S. (1977). *Zh. Prikl. Khim.* USSR.

Kanury, A. M. (1982). In *Introduction to Combustion Phenomena.* Gordon and Breach, New York, Chapter 7.

Kauppinen, E. I., and Pakkanen, T. A. (1990). *Atmos. Environ.* 24A:423.

Kowalczyk, G. S., Choquette, C. E., and Gordon, G. E. (1978). *Atmos. Environ.* 12:1143.

Law, S. L., and Gordon, G. E. (1979). *Environ. Sci. Technol.* 13:432.

Lee, C. C. (1988). *J. Air Pollut. Control Assoc.* 38:941.

Lee, K. W., and Chen, H. (1984). *Aerosol Sci. Technol.* 3:327.

Moore, J. W., and Pearson, R. G. (1981). *Kinetics and Mechanism.* John Wiley & Sons, New York, Chapter 4.

Mulholland, J. A., and Sarofim, A. F. (1991). *Environ. Sci. Technol.* 25:268.

Oppelt, E. T. (1986). *Environ. Sci. Technol.* 20:312.

Oppelt, E. T. (1987). *J. Air Pollut. Control Assoc.* 37:558.

Pratsinis, S. E. (1988). *J. Colloid Interface Sci.* 124:416.

Sethi, V. (1990). M.S. Thesis. University of Cincinnati, Cincinnati, OH.

Sethi, V., and Biswas, P. (1990a). *J. Air Waste Manage. Assoc.* 40:42.

Sethi, V., and Biswas, P. (1990b). *Proceedings of the Sixteenth Annual Hazardous Waste Research Symposium,* EPA 600/9-90/037, pp. 59–67.

Smith, R. D., Campbell, J. A., and Neilson, K. K. (1979). *Am. Chem. Soc.* 13:553.

Vogg, H., Braun, H., Metzger, M., and Schneider, J. (1986). *Waste Manage. Res.* 4:65.

Waterland, L. R., Fournier, D. J., Whitworth, W. E., and Carroll, G. J. (1990). Presented at AAAR Annual Meeting, Philadelphia, p. 221.

Received August 30, 1991; accepted February 3, 1992.